Composition of trioctahedral micas in the Karlovy Vary pluton, Czech Republic and a comparison with those in the Cornubian batholith, SW England

M. STONE

Earth Resources Centre, University of Exeter, Exeter EX4 4QE, UK

J. KLOMÍNSKÝ

Czech Geological Survey, Klárov 3, 118 21 Prague 1, Czech Republic

AND

G. S. RAJPOOT

Konevova 110, 13000 Prague 3, Czech Republic

Abstract

Trioctahedral micas in the Karlovy Vary pluton range in composition from Fe-biotites in the granites of the Older Intrusive Complex (OIC) through siderophyllite and lithian siderophyllite to zinnwaldite in the granites of the Younger Intrusive Complex (YIC). Li + Al^{VI} + Si would appear to substitute for Fe^{2+} + Al^{IV} in biotite with a formula similar to that given in Henderson *et al.* (1989), but Li + Si appears to substitute for Fe^{2+} + Al^{IV} in the Li-micas. In mica *vs.* host rock plots, Rb and F show positive linear covariation except for the Li-mica granites, but femic constituents and tFeO/(tFeO + MgO) have separate trends for OIC and YIC granites and micas. Further differences between OIC and YIC granite micas are seen in their Ti and Mg contents and in plots like V *vs.* SiO_2, Al^{IV} *vs.* Fe/(Fe+Mg) and Li *vs.* total iron as Fe^{2+} and in the results of discriminant analysis. These reveal a geochemical hiatus between OIC and YIC granite micas that coincides with a major temporal hiatus.

Biotite compositions in the YIC granites are similar to those in the granites of the Cornubian batholith and reveal a similar magmatic evolution and genesis in which later biotites evolve to lithian siderophyllites with some enrichment in trace alkalis and F. It is suggested that the biotite granites in the YIC were derived from the products of partial fusion of the OIC granites. A less well-marked geochemical hiatus exists between YIC biotites and zinnwaldites. In some plots (e.g. Si *vs.* Li, Li *vs.* tFe) apparent continuity between biotite and the Li-micas suggests continuous evolution, but in others (e.g. Rb *vs.* TiO_2 , Rb(biotite) *vs.* Rb(rock)), Li-mica data points stand apart from the biotites suggesting, like the whole rock data, a separate evolution. Comparison with the more abundant data for Li-micas of the Cornubian batholith suggests derivation of the Li-mica granites by partial fusion of the OIC/YIC granite residues.

KEYWORDS: trioctahedral micas, granites, Karlovy Vary pluton, Cornubian batholith.

Introduction

THE Karlovy Vary pluton is the largest granite body (area *c.* 1000 km^2) in the Krušné hory–Smrčiny batholith in the west Bohemian Massif and continues into Germany as part of the Erzgebirge province. The granites are Upper Carboniferous to Lower Permian in age and consist of an Older Intrusive Complex (OIC) and a Younger Intrusive Complex (YIC) (Lange *et al.*, 1972). According to Tischendorf (1989), the OIC granites give ages of 330–320 Ma whilst the YIC granites are some 25 Ma later at

Mineralogical Magazine, December 1997, Vol. 61, pp. 791–807

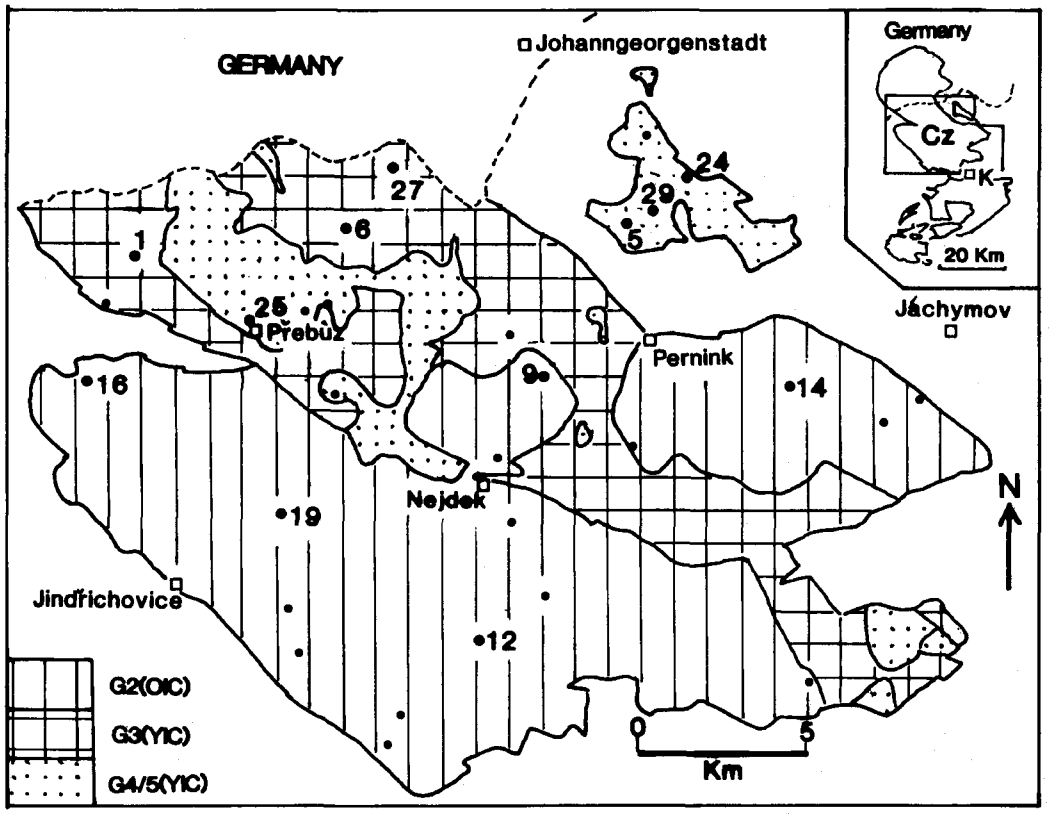

FIG. 1. Map of the Czech part of the Karlovy Vary pluton showing distribution of the main granite types and sample locations (filled circles). Numbered sample locations (larger filled circles) correspond with numbered representative samples in Tables 1 and 3. Older Intrusive Complex (OIC) G2 granite and Younger Intrusive Complex G3 to G5 granites as described in the text. The dashed line is the border between Germany and the Czech Republic. In inset K = Karlovy Vary, Cz = Czech Republic.

305–295 Ma, although seven Rb-Sr isochrons given in Gerstenberger (1989) indicate ages ranging from 324 to 305 Ma, with marked overlap between those of OIC and YIC granites. The central part of the Karlovy Vary pluton crops out within Czech territory and is composed of about equal amounts of both OIC and YIC complexes (Fig. 1). Several granite types have been distinguished (Lange *et al.*, 1972; Klomínský and Absolonová, 1974; Štemprok, 1986; Tischendorf, 1989): the nomenclature used here is that given by Rajpoot and Klomínský (1994). The OIC is represented by the G2 granites (mesocratic, two-mica, coarse- to medium-grained, poorly fractionated, post-tectonic, tin-barren, peraluminous monzo- to syenogranites) and the YIC mainly by G3 and G4 granites and subordinate G5 granites. The G3 and G4 are leucocratic, two-mica, post-orogenic syenogranites, but, whereas the former are coarse-grained, moderately differentiated, peraluminous and partly stanniferous, the G4 granites, which generally contain significant topaz, are medium- to fine-grained, more strongly differentiated, stanniferous and highly peraluminous. The G5 granites characteristically contain Li-mica and topaz, are medium- to fine-grained, leucocratic, stanniferous, alkali-rich and highly peraluminous. In addition, early hybrid porphyritic biotite granites contaminated by pelitic country rocks (herein called G3*) form enclaves in the G3 and G4 granites.

Trioctahedral micas from the German part the of the batholith have already been studied (Müller, 1966; Bauer, 1967; Tischendorf *et al.*, 1969; Gottesman and Tischendorf, 1978; Hecht, 1994) and special attention has been paid to their role as

indicators of tin mineralization. Those in the G2 granites are Fe-biotites, but in the YIC (G3-G5) they range widely in composition to Li-bearing siderophyllite and protolithionite (zinnwaldite) in some G4 and G5 granites (Tischendorf *et al.*, 1969).

In this study, the chemistry of the trioctahedral micas in the Czech part of the batholith has been studied with a view to determining their compositions in each of the granite types, the extent and type of atomic substitution and their magmatic evolution. Comparisons are made with the chemistry of the host granites and with micas from similar Variscan granites of the Cornubian batholith of SW England. Thirty samples of trioctahedral mica and host granite were analysed for major element oxides and several trace elements (Fig. 1; Tables 1 and 3). Micas were preconcentrated by means of a shaking table and further cleaning was done in acetylene tetrabromide followed by magnetic separation. Chemical analyses were carried out in the laboratories of the Czech Geological Survey, Prague.

Trioctahedral mica chemistry

Chemical data. Trioctahedral mica compositions (Table 1) compare with those from other European Variscan S-type granites in having high contents of Li_2O, F and Sn and in ranging in composition from Fe-Mg biotite into zinnwaldite. These features contrast with biotites from typical I-type granites such as those in the Caledonian of the British Isles: these have low Li_2O and F and higher MgO (e.g. Haslam, 1968; Leake, 1974; Weiss and Troll, 1989) and typically do not show marked Li enrichment in the more evolved granites. The correlation matrix of raw data for the Karlovy Vary micas (Table 2) reveals two strongly associated groups of constituents, namely, the 'femic' elements (TiO_2, MgO, FeO and CaO) and the 'F - alkali' elements (F, Rb_2O, Li_2O, K_2O, Sn, SiO_2). Clearly, variation diagrams for elements taken from one or other of these suites will show positive covariation, e.g. Li_2O *vs.* SiO_2 (Fig. 2*a*), but elements taken, one from each of the two suites, e.g. Rb *vs.* TiO_2 (Fig. 2*b*) and V *vs.* SiO_2 (Fig. 2*c*), show negative covariation. The first two (Fig. 2*a* and *b*) compare with patterns published for data from the Cornubian batholith (Stone *et al.*, 1988; Henderson *et al.*, 1989), referred to below. In Fig. 2*c*, data points for biotites from the G2 granites plot well apart from those of the other micas, a recurrent feature noted below. In general, these relations show a decrease in the 'femic' element association and increase in the 'alkali-F' association in the time sequence of granite emplacement, G2 to G5. This, together with the obvious substitution between Si and Al^{IV} yet significant positive correlation between Al_2O_3 and SiO_2 , leads to a predicted substitution $Li (+ Al^{VI}) + Si = Al^{IV} + R^{2+}$ examined in more detail below. Formulae have been calculated on the basis of 22 oxygen atoms (Table 1). Octahedral sites contain > 5 cations, thereby confirming the trioctahedral nature of the micas. The interlayer cations commonly sum to < 2 (range from 1.42 to 2.13) that could be the result of post-magmatic leaching and/or H_3O^+ ion substitution (Chaudhry and Howie, 1973).

Petrographic occurrence. Initial examination of the raw and formula data (Table 1) and plots of means and confidence limits for formula data clearly differentiate the biotites of the OIC and YIC granites. For example, Ti (Fig. 3*a*), like Mg (Fig. 3*b*), tFe (total Fe as Fe^{2+}) (Fig. 3*c*), Ni, V and Co (i.e. the 'femic-element' suite) are higher in the micas of the OIC (G2) granites compared with those in the YIC granites. On the other hand, Si, Al, K, Li (Fig. 3*e*), F (Fig. 3*d*) and Rb (the 'fluoride-alkali' suite) are distinctly higher in the micas of the younger granites. Data for the G4 and G5 granites have been combined in Fig. 3*a,b,d* and *f* owing to the small number of samples. However, the G5 granite micas stand apart from those in the other YIC granites in having very low total iron (tFe, Fig. 3*c*), Mg and V, but significantly higher Rb, Li (Fig. 3*e*) and F. Patterns are similar whether the G3* enclaves (i.e. the oldest of the YIC granites) are included with the G3 granites or omitted.

Several parameters in Fig. 3 show 'progressive' changes in mica composition with change in rock type from G2 to G5. For example, Si, F (Fig. 3*d*), Li (Fig. 3*e*) and Rb show increases, whilst Al^{IV} (which must decrease as Si increases), Ti and tFe^{2+} (Fig. 3*a* and *c*) decrease in the sequence. Some parameters, like Mg (Fig. 3*b*) and $(Fe^{2+} + Fe^{3+})/(Fe^{2+} + Fe^{3+} + Mg)$, referred to subsequently as #Fe (Fig. 3*f*), show trends from a completely isolated G2 to a more composite YIC biotite composition field.

There is good positive covariation in Li *vs.* F (Fig. 4*a*), Li *vs.* Rb, F *vs.* Al^{VI} and Al^{VI} *vs.* #Fe (Fig. 4*b*), although in some plots (not shown), e.g. F *vs.* Al^{VI} and F *vs.* Al^{IV} , and in Li *vs.* total Al (Fig. 4*d*), the G5 granite micas tend to stand apart from the linear variation. In Fig. 4*d*, the G5 granite micas follow a trend similar to that in the Al_2O_3 *vs.* Li_2O diagram in Henderson *et al.* (1989, Fig. 2*b*). The Al^{IV} *vs.* #Fe (Fig. 4*c*) plot clearly separates the G2 granite biotites from the others; the latter trend towards $Al^{IV} = 1$ with concomitant increase in Si as #Fe approaches 1. The Al^{VI} *vs.* #Fe (Fig. 4*b*) plot does not discriminate between the G3, G4 and G5 granite micas; the G3* micas partially link the YIC granite micas with the well-separated G2 granite biotites to give an overall trend in time towards high Al^{VI} coupled with high #Fe. The Fe^{2+} *vs.* Mg plot (Fig. 4*e*) shows a strong association in the YIC granites (correlation coefficient, r = +0.74· Fe^{2+} =

TABLE 1. Representative chemical analyses of trioctahedral micas

	1 G*	5 G5	6 G5	9 G2	12 G2	14 G2	16 G2	19 G2	24 G4	25 G4	27 G3	29 G3
wt.%												
SiO_2	37.68	47.69	39.36	34.92	35.02	35.56	34.42	33.38	39.40	36.72	38.72	38.79
TiO_2	2.36	0.55	0.88	3.10	3.66	4.20	3.95	3.40	1.01	0.60	1.46	1.30
Al_2O_3	20.58	20.20	23.42	17.70	18.21	14.41	17.49	19.00	25.56	22.41	22.10	22.44
Fe_2O_3	1.98	0.38	0.55	2.58	3.31	2.64	3.16	3.26	5.72	3.10	1.82	2.25
FeO	19.80	9.84	15.82	18.20	17.42	17.84	18.10	17.71	11.00	17.80	16.92	16.60
MnO	0.27	0.35	0.35	0.30	0.38	0.37	0.36	0.41	0.19	0.41	0.31	0.26
MgO	2.68	0.51	0.68	8.40	7.08	9.49	7.97	6.53	0.83	1.74	1.54	1.56
CaO	0.28	0.98	0.34	0.35	0.84	1.13	0.63	0.84	0.41	0.16	1.12	0.31
Na_2O	0.30	0.32	0.30	0.50	0.33	0.23	0.21	0.22	0.58	0.26	0.24	0.22
K_2O	8.88	11.04	10.66	7.80	8.55	9.24	9.09	8.26	6.68	9.94	9.60	9.94
Li_2O	0.66	4.21	1.64	0.24	0.25	0.12	0.22	0.36	1.02	0.99	1.07	0.87
P_2O_5	0.22	0.68	0.12	0.31	0.40	0.67	0.33	0.52	0.34	0.08	0.08	0.16
F	2.61	7.86	4.18	1.04	0.71	0.56	0.60	0.74	3.94	3.09	2.53	3.06
	98.30	104.61	98.30	95.44	96.16	96.46	96.53	94.63	96.68	97.30	97.51	97.76
-O=F	1.10	3.31	1.76	0.44	0.30	0.24	0.25	0.31	1.66	1.30	1.07	1.29
Total	97.20	101.30	96.54	95.00	95.86	96.22	96.28	94.32	95.02	96.00	96.44	96.47
ppm												
Rb	288	880	–	97	93	71	95	102	370	–	–	428
Sn	75	660	140	64	49	33	56	56	85	83	450	220
Zn	420	340	270	270	190	180	180	250	280	350	470	340
Ni	13	2	12	19	38	46	35	40	2	5	13	3
V	38	11	8	180	210	230	180	150	15	40	30	18
Formulae on basis of 22 oxygen atoms												
Si	5.693	6.658	5.883	5.386	5.368	5.513	5.286	5.269	5.800	5.613	5.792	5.821
Al^{IV}	2.307	1.342	2.117	2.614	2.632	2.487	2.714	2.731	2.200	2.387	2.208	2.179
Al^{VI}	1.358	1.982	2.009	0.603	0.657	0.147	0.452	0.754	2.235	1.650	1.689	1.790
Ti	0.268	0.058	0.099	0.360	0.422	0.490	0.456	0.398	0.111	0.069	0.164	0.147
Fe^{3+}	0.225	0.040	0.062	0.299	0.382	0.308	0.365	0.382	0.634	0.357	0.205	0.254
Fe^{2+}	2.502	1.149	1.977	2.347	2.233	2.313	2.325	2.305	1.354	2.275	2.117	2.083
Mn	0.035	0.041	0.044	0.039	0.049	0.049	0.047	0.054	0.024	0.053	0.039	0.033
Mg	0.604	0.106	0.151	1.931	1.618	2.193	1.824	1.515	0.182	0.396	0.343	0.349
Li	0.401	2.364	0.986	0.149	0.154	0.075	0.136	0.225	0.604	0.609	0.644	0.525
ΣY	5.393	5.740	5.328	5.728	5.515	5.574	5.606	5.633	5.144	5.409	5.201	5.181
Ca	0.000	0.013	0.029	0.000	0.051	0.041	0.032	0.026	0.000	0.009	0.162	0.016
Na	0.088	0.087	0.087	0.150	0.098	0.069	0.063	0.066	0.166	0.077	0.070	0.064
K	1.712	1.966	2.032	1.535	1.672	1.827	1.781	1.640	1.254	1.938	1.832	1.903
Rb	0.003	0.009	–	0.001	0.001	0.001	0.001	0.001	0.004	–	–	0.005
X	1.803	2.074	2.149	1.685	1.822	1.938	1.877	1.733	1.424	2.024	2.064	1.987
F	1.247	3.471	1.976	0.507	0.344	0.275	0.291	0.364	1.834	1.494	1.197	1.452

G* = G3* granite enclaves. G2, G3, G4, G5 as in text. – not determined. Al^{IV} and Al^{VI} – tetrahedral and octahedral Al respectively. ΣX and ΣY – sums of X and Y sites respectively.

2.95Mg + 1.20), but a weak negative relationship in micas from the OIC granites and contaminated enclaves (r = −0.21; Fe^{2+} = −0.04Mg + 2.41), although OIC granite micas again are separated from all the others. The OIC data plot firmly on the experimental Ni–NiO curve in the Fe^{3+}–Fe^{2+}–Mg

TABLE 2. Pearson product-moment correlation matrix of raw mica data

	SiO_2	TiO_2	Al_2O_3	tFeO	MnO	MgO	CaO	Na_2O	K_2O	Li_2O	Rb	F
TiO_2	−0.80											
Al_2O_3	+0.54	−0.89	–									
tFeO	−0.88	**+0.64**	−0.44	–								
MnO	−0.29	+0.22	−0.21	+0.35	–							
MgO	−0.76	**+0.96**	−0.92	+0.55	+0.16	–						
CaO	−0.18	+0.48	−0.51	−0.08	+0.03	+0.48	–					
Na_2O	+0.29	−0.33	+0.36	−0.42	−0.44	−0.23	0.00	–				
K_2O	**+0.63**	−0.50	+0.19	−0.39	−0.08	−0.48	−0.31	−0.27	–			
Li_2O	**+0.94**	−0.75	+0.49	−0.74	−0.24	−0.70	−0.14	+0.19	**+0.62**	–		
Rb	**+0.78**	−0.57	+0.41	−0.74	−0.38	−0.54	−0.20	+0.30	+0.36	**+0.81**	–	
F	**+0.95**	−0.89	**+0.69**	−0.86	−0.30	−0.85	−0.27	+0.34	+0.56	**+0.95**	**+0.80**	–
Sn	**+0.58**	−0.42	+0.21	−0.56	−0.01	−0.35	−0.05	−0.07	+0.35	**+0.62**	+0.51	+0.53

Positive values significant at the 0.01 level are underlined ($r > 0.46$), those significant at the 0.001 level are shown in bold type ($r > 0.57$). Values based upon the t-distribution with 28 degrees of freedom. tFeO = total iron as FeO.

triangle (cf. Speer, 1984), but YIC micas plot much closer to the Fe^{2+} apex and show much wider scatter, perhaps indicating heterogeneous post-magmatic re-equilibration.

Multiple discriminant analysis using the raw major element data and grouping together the G5 and G4 granite micas, because of an insufficient number of samples in each group, results in a clear classification into G2, G3 and G4/5 granite micas. The squared distance (d^2 or Mahalanobis distance, a measure of separation between multivariate means) between the three groups indicates that the OIC (G2) granite biotites differ markedly from the YIC granite micas and that the differences between G3 and G4/5 micas are much less, thereby convincingly supporting the evidence for a geochemical hiatus between OIC and YIC granite micas in the univariate and bivariate plots given above.

Host-granite compositional relationships. Representative analyses of the host granites of the analysed micas are given in Table 3. Variation diagrams (not shown) between oxides/elements of the 'femic' suite, viz. TiO_2, MgO, FeO, CaO, Zr, Sr, Ba and Th, tend to separate the G2 granites from the rest, and plots involving Li and Sn tend to separate the G5 granites. The correlation matrix (not shown) reveals a strong femic association (TiO_2, MgO, FeO, CaO, Zr, Sr, Ba and Th) and also an important F-Rb-Li-Sn association and is typical of many granite suites, especially those in which later members are enriched in Li and Sn, such as the Cornubian granites of SW England. The rock correlations are broadly similar to those of their trioctahedral micas, with positively correlated femic constituents (TiO_2, FeO, MgO, plus CaO, Zr, Sr, Ba and Th) on the one hand and trace alkalies (Li, Rb) and F (plus SiO_2 and P_2O_5) on the other. Obviously, this would lead to expected positive correlations of these oxides/elements between mica and rock, especially for MgO and Li (for which the mica may be the sole host) as, indeed, is the case (Table 4).

In detail, plots of biotite *vs.* rock for TiO_2, FeO and MgO are more complex and reveal two data sets. For example, small amounts of MgO in rocks containing biotite as their only MgO-bearing mineral have data points in an MgO(biotite) *vs.* MgO(rock) plot that define a set of linear trends that pass through or close to the origin. The slope of each such line is a function of the amount of biotite in the rock but as most granites contain some 3–10 per cent of biotite (by volume), we would expect data points that theoretically lie on slightly different lines to appear to be almost linear. A regression line for the YIC granites (i.e. those with low MgO) alone (Fig. 5*a*) passes close to the origin and has a slope, m = 11.0 that corresponds with *c.* 8% of biotite (by volume). The reduced major axis (which bisects the Y on X and the X on Y regression lines) is steeper (m = 13.6), equivalent to a more realistic < 6.5 vol. % of biotite. Some of the sixteen OIC granite samples lie on this line, but overall they, and an additional 170 partial analyses, also define another line that intersects the steeper regression line at ~0.7% MgO(rock). The lower slope of the OIC granite line results from larger amounts of biotite accounting for the MgO(rock) and/or the presence of additional Mg-bearing

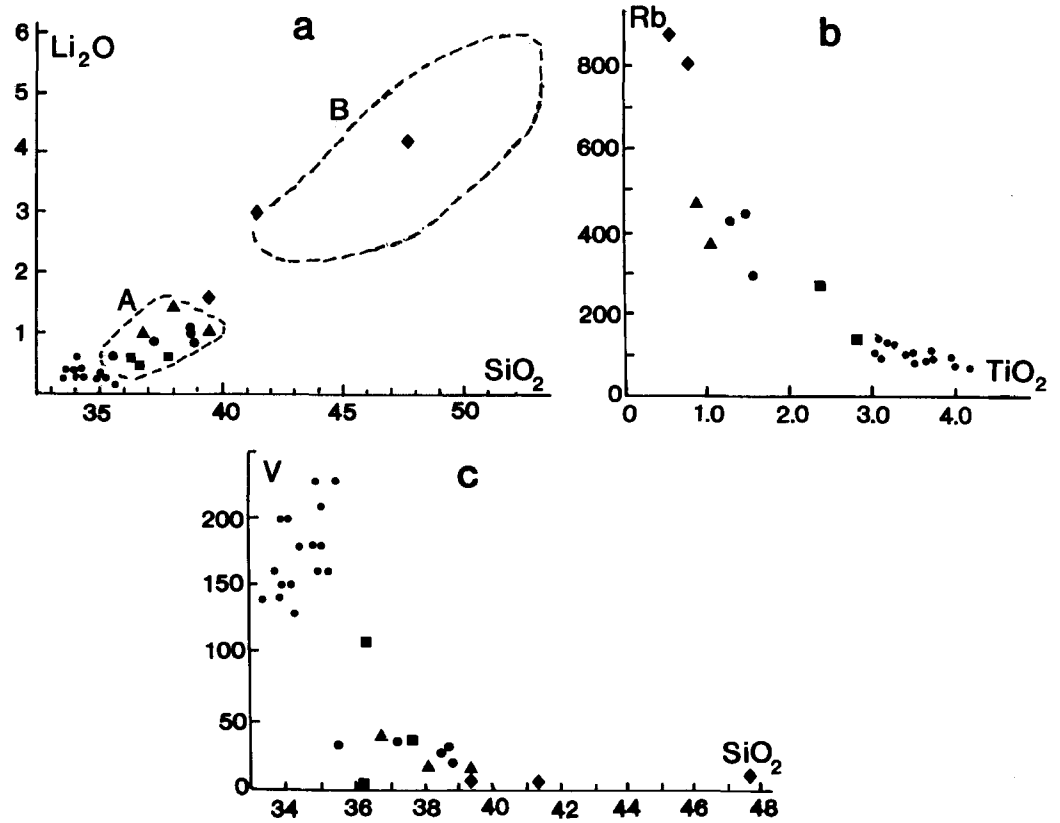

FIG. 2. Bivariate plots of raw data for trioctahedral micas: (*a*) Li_2O (wt.%) *vs.* SiO_2 (wt.%); (*b*) Rb (ppm) *vs.* TiO_2 (wt.%); (*c*) V (ppm) *vs.* SiO_2 (wt.%). Small filled circles = G2 granite micas; filled squares = G3* micas; large filled circles = G3 micas; filled triangles = G4 micas; filled diamonds = G5 micas. In Fig. 2*a*, composition field A (enclosed by dashed line) = biotite in Cornubian Type B granites and B = Li-micas from the Tregonning (Stone *et al.*, 1988) and St. Austell granites (Henderson *et al.*, 1989).

minerals such as hornblende. Similar patterns are shown by both FeO and TiO_2 although, unlike MgO, even at low contents, both these oxides are contained in other (accessory) minerals.

Strong positive mica–rock correlations (i.e. associations), combined with an elongate spread of data points along lines of best fit, in Al^{VI} *vs.* F(rock) (+0.79) and the ratio tFe/(tFe+Mg) (+0.80) reflect close fits to the regression lines. Additional associations occur in Li_2O (+0.49), Al^{VI} *vs.* aluminium saturation index or ASI (rock) (+0.50) and Al^{VI} *vs.* SiO_2 (rock) (+0.51). However, in some plots, such as those for Rb (Fig. 5*c*) and F, the G5 granites are far removed from the regression lines. The high correlations for Rb (+0.92) and F (+0.97), with the three G5 granites deleted, are consistent with their prominence in trioctahedral micas.

Tin in micas and rocks. Plots for Sn in Karlovy Vary micas and rocks (Fig. 5*b*) show a wide scatter of data points. The regression line in Fig. 5*b*, based upon 24 analysed mica and rock samples (five were rejected by Minitab), is markedly influenced by the two data points with high values in both mica and rock. Data points that lie well above this line may indicate lower biotite contents and/or higher concentrations of Sn in biotite, perhaps associated with the occurrence of cassiterite inclusions in biotite, whereas those that lie well below this indicate free cassiterite in the host rock. The percentage of total Sn in the rock contained in biotite (in solution and as inclusions) is readily estimated from the Sn contents of mica and rock and the amount of biotite. Biotites in granites from northern Portugal investigated by Neiva (1976) contain a maximum of 21% of the total

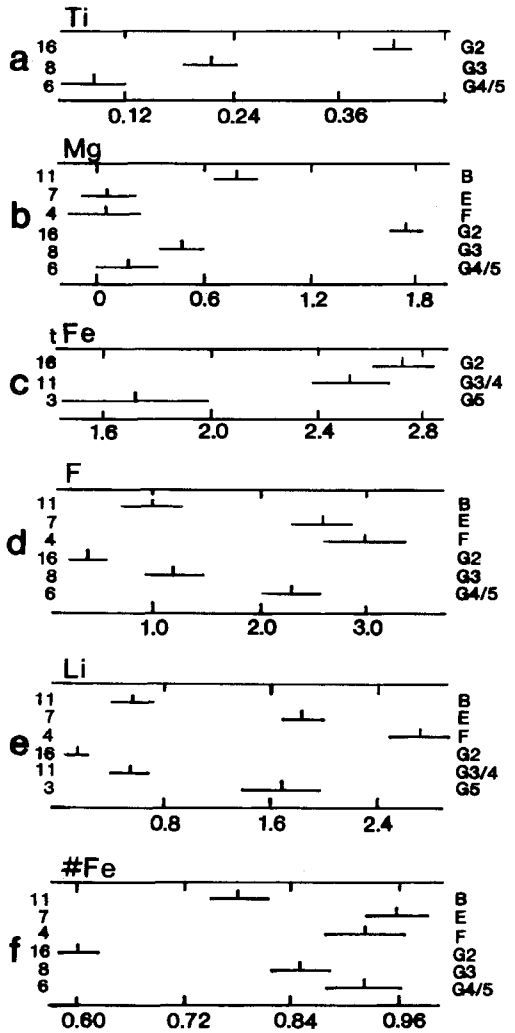

FIG. 3. Atomic means (based upon 22 oxygen atoms) and 95% confidence intervals for trioctahedral micas. (*a*) Ti and (*c*) tFe (i.e. total Fe as Fe^{2+}) include micas from the Karlovy Vary pluton only. The others, (*b*) Mg, (*d*) F, (*e*) Li and (*f*) #Fe (i.e. tFe/(tFe+Mg)) also include Cornubian micas from Stone *et al.* (1988). Numbers on the left margin of each figure give the number of analyses. On the right margin - G2, G3, G4 and G5 are Karlovy Vary micas as described in the text: B = biotite from megacrystic biotite granite, E = zinnwaldite from aphyric zinnwaldite-albite-topaz granite and F = lepidolite from lepidolite-albite-topaz roof differentiates of E in the Cornubian batholith.

Sn. On the assumption of 5% biotite in the Karlovy Vary rocks, the amount of the total Sn contained in biotite averages at *c.* 20%, but with a wide range of 16–59% and higher values prominent in G5 zinnwaldites. As in the case of MgO, data points that lie close to the regression line at low Sn contents could reflect solubility of Sn in biotite, although some Sn may occur as submicroscopic inclusions of cassiterite. This would not be revealed by the Portuguese or Czech data as the analyses were done on biotite separates.

The Sn contents of Cornubian biotites given in Stone *et al.* (1988) range from 9–76 ppm, but with typical values of 30–50 ppm, whilst Li-micas have typical Sn contents up to 80 ppm. As in the case of the Karlovy Vary micas, these analyses were obtained from mica concentrates. A subsequent preliminary electron microprobe investigation points to some variability within Cornubian samples, as expected at low detection limits, but indicates that Sn contents in both siderophyllites and Li-micas are typically less than 100 ppm (Table 5). Actual values range from zero to <50 ppm in basic microgranite (Type A) inclusions in both the Land's End and Dartmoor granites and up to 100 ppm in the Type B granites of the Carnmenellis pluton and several hundred ppm in the more evolved granites and microgranites. Within-specimen consistency of these higher values suggests that the Sn is contained in the biotite structure (at least up to a recorded 750 ppm). Typically low contents in the Li-micas compare with most biotites, but occasionally markedly erratic values (e.g. from 0–500 ppm in a zinnwaldite in one sample - and 0 ppm generally, but one value of >5000 ppm in a muscovite) points to localized concentrations of Sn that are likely to be submicroscopic inclusions of cassiterite.

Maps of the distribution of Sn, Li and F in trioctahedral micas of the YIC granites (not shown), drawn by simple contouring using a large number of sample points, show broad correspondence between 'high' points which, in turn, reflect the already observed high positive correlation coefficients between these elements. There is also a broad negative relationship between the distributions of these elements and Mg (not illustrated) in the micas. Location of known Sn greisen deposits is broadly controlled by altitude and, therefore, proximity to the roof, and is associated with positive anomalies of Sn, Li and F in the micas. In the case of Sn, 15 out of 22 deposits lie within the >100 ppm contour and for Li, 21 deposits lie within the >80 ppm contour, whilst for F, 18 deposits lie within the >2.5 wt.% contour. In all cases, the OIC granite micas have considerably lower contents of these elements. Such anomalies point to the practicability of using Sn and Li in such micas in prospecting for greisen-style tin deposits.

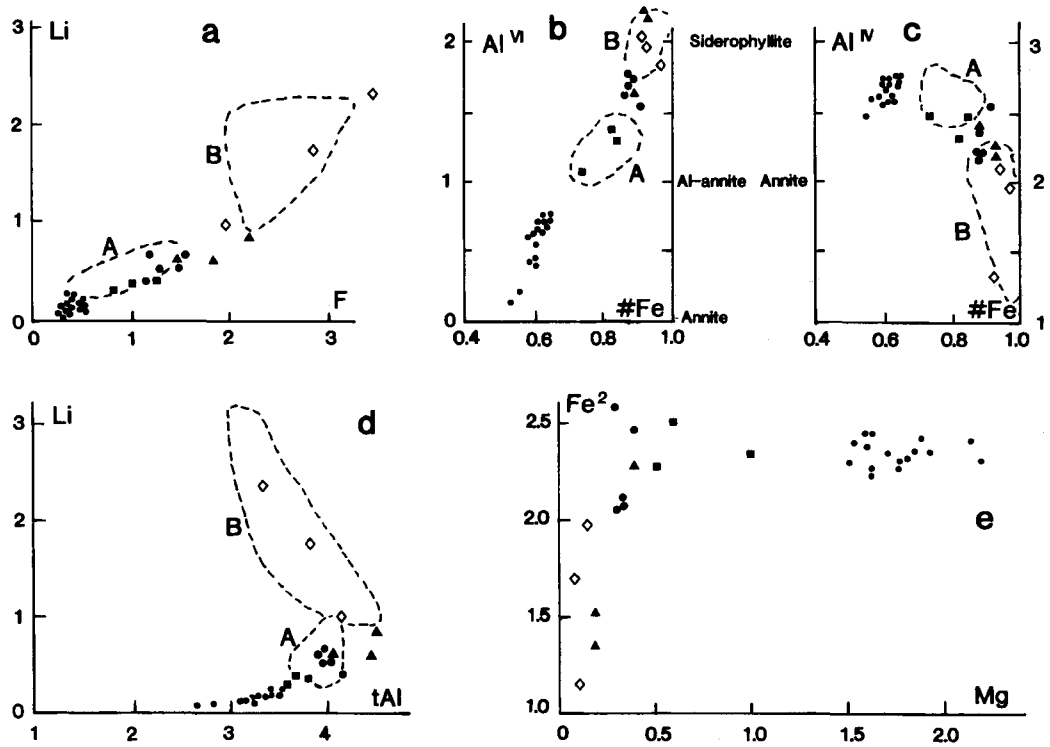

FIG. 4. Bivariate formula plots (based upon 22 oxygen atoms) of trioctahedral mica compositions. (*a*) Li *vs.* F, (*b*) Al^{VI} *vs.* #Fe, (*c*) Al^{IV} *vs.* #Fe, (*d*) Li *vs.* tAl, (*e*) Fe^{2+} *vs.* Mg. Symbols as in Fig. 2 but with open diamonds = G5 micas, #Fe as in Fig. 3. Composition fields of Cornubian micas outlined by dashes, A = biotites from megacrystic biotite granite, B = zinnwaldites from Li-mica granite (data from Stone *et al.*, 1988).

Formulae and substitution. A plot of formula compositions on the octahedral cation Li–Al (+ Fe^{3+} + Ti)–Fe^{2+} (+Mn) triangle of Foster (1960) gives a generalized trend from Fe^{2+}-rich biotites to typical siderophyllites which extend to the edge of the zinnwaldite field (Fig. 6). Two of the three G5 micas lie within the zinnwaldite field but plot away from the general biotite trend. The fields shown in Fig. 6 are those proposed by Stone *et al.* (1988) who divide the Li-Fe micas, based upon Li content of the unit cell, as follows: siderophyllite < 1 (lithian siderophyllite > 0.5 but < 1.0); zinnwaldite 1.0–2.5; and lepidolite > 2.5. This provides a compromise between the classifications proposed by Foster (1960) and Rieder (1970), like that given for the trioctahedral micas of the Cornubian batholith (Stone *et al.*, 1988) referred to below. In Fig. 6, data points for the G2 granite micas lie close to the composition point of Al-annite (on the R^{3+}–R^{2+} sideline at *c.* 80% R^{2+}), as they do also in Fig. 7*b* (Si *vs.* Li, close to Si = 5, Li = 0). In Fig. 4*b* (Al^{VI} *vs.* #Fe), they plot as Fe biotites with #Fe > 0.5 and Al^{VI} < 1. On the other hand, G3 and G4 granite micas are typical siderophyllites in Fig. 6 (also in Fig. 4*b*). G5 granite micas are zinnwaldites.

The term siderophyllite is used here for biotites that have Al^{VI} > 1, #Fe > 0.5 and Li < 1 (lithian siderophyllites have Li > 0.5 but < 1). The general formula

$$K_2R^{2+}_xLi_{4-x}R^{3+}_2(Al_xSi_{8-x})O_{20}(OH,F)_4$$

applies to the Li-Fe micas described by Foster (1960), Rieder (1970) and Stone *et al.* (1988). Whilst approximately applicable to our YIC granite micas, it does not take into account octahedral vacancies (i.e. samples with < 6 octahedral cations in the formula) and those with R^{3+} > 2, or include samples with $R^{3+} \ll 2$ (as in the G2 granite biotites). R^{2+} + Li ranges from *c.* 2.2 (in G4 granite micas) to >4 (in G2 granite micas), R^{3+} is close to 2 in the G3*, G3 and G5 micas, ranges up to 3 in G4 and is typically between 1 and 1.5 in G2 micas. Total

TABLE 3. Representative analyses of Karlovy Vary granitoids

	1 G*	5 G5	6 G5	9 G2	12 G2	14 G2	16 G2	19 G2	24 G4	25 G4	27 G3	29 G3
wt.%												
SiO_2	74.76	–	74.38	72.30	70.69	64.39	71.22	71.25	–	74.60	74.90	74.03
TiO_2	0.40	0.10	0.05	0.40	0.40	0.56	0.34	0.22	0.06	0.10	0.10	0.08
Al_2O_3	13.41	–	14.03	13.70	14.12	15.37	14.68	14.11	–	13.57	13.59	13.92
Fe_2O_3	0.86	–	0.26	0.67	0.49	0.82	0.70	0.54	–	0.56	0.49	0.59
FeO	1.08	–	0.87	1.90	2.01	3.00	2.26	1.58	–	1.14	0.86	0.79
MgO	0.26	0.14	0.14	0.85	1.06	2.35	0.70	0.45	0.14	0.22	0.14	0.12
CaO	0.80	0.47	0.89	0.99	1.22	0.90	1.28	0.69	0.49	0.42	0.41	0.34
Na_2O	3.68	3.04	2.95	3.45	3.45	3.59	3.60	3.14	2.98	3.25	2.93	3.17
K_2O	3.20	4.88	4.84	4.61	4.86	4.79	4.40	4.63	5.25	4.53	4.73	4.94
P_2O_5	0.14	0.24	0.15	0.19	0.14	0.18	0.16	0.13	0.25	0.27	0.27	0.22
F	0.43	0.55	0.40	0.09	0.06	0.06	0.06	0.04	0.67	0.44	0.46	0.44
	99.02		98.96	99.15	98.50	96.01	99.40	96.78		99.10	98.88	98.64
-O=F	0.18		0.17	0.04	0.03	0.03	0.03	0.02		0.19	0.19	0.19
Total	98.84		98.79	99.11	98.47	95.98	99.37	96.76		98.91	98.69	98.45
ppm												
Li	46	372	1208	158	136	418	139	232	604	460	302	278
Rb	560	770	–	310	240	230	270	280	910	684	740	720
Sn	32	77	–	18	24	21	44	25	59	29	61	31
Sr	40	26	35	126	163	375	247	96	27	30	24	29
Ba	251	37	12	439	385	780	385	257	47	39	80	29
U	13	7	–	4	7	5	6	7	9	–	14	33
Th	17	11	–	22	22	24	25	11	6	–	13	10
Zr	240	35	33	170	155	285	165	95	10	88	55	30

– not determined

G2, G3*, G3, G4 and G5 and column numbers as in Table 1.

octahedral sites lie fairly close to 5.5 (range here 5.15–5.87). Thus, on the basis of all data given above we can classify the OIC granite micas as Fe-biotites (Li <0.5, $Al^{VI} < 1$, #Fe > 0.5), whilst the YIC granite micas range from siderophyllite through lithian siderophyllite (in G3 and G4 micas respectively) to zinnwaldite (Li>1<2.5, $Al^{VI} > 1$, #Fe>0.5) in the G5 granite micas.

In the Li *vs.* tFe diagram (Fig. 7*a*), the overall pattern is one of negative covariation, like that given in Stone *et al.* (1988, Fig. 5*a*), although the data of Henderson *et al.* (1989), mainly from the St. Austell granite, give a slightly steeper line. Stone *et al.* (1988) conclude that the substitution ratio between Li and Fe^{2+} is close to 1:1, in which case the coupled substitution $Li^{VI} + Si^{IV} = (Fe^{2+})^{VI} + Al^{IV}$ might operate (Henderson *et al.*, 1989, equation 1, p. 437):

TABLE 4. Mica–rock correlation coefficients (r)

	r	n
TiO_2	+0.86	29
Fe_2O_3	+0.54	19
tFeO	+0.68	19
MgO	+0.81	30
Li_2O	+0.88	30
Rb_2O	+0.87	29
Sn	+0.42	29
F	+0.85	30

n = no. of samples

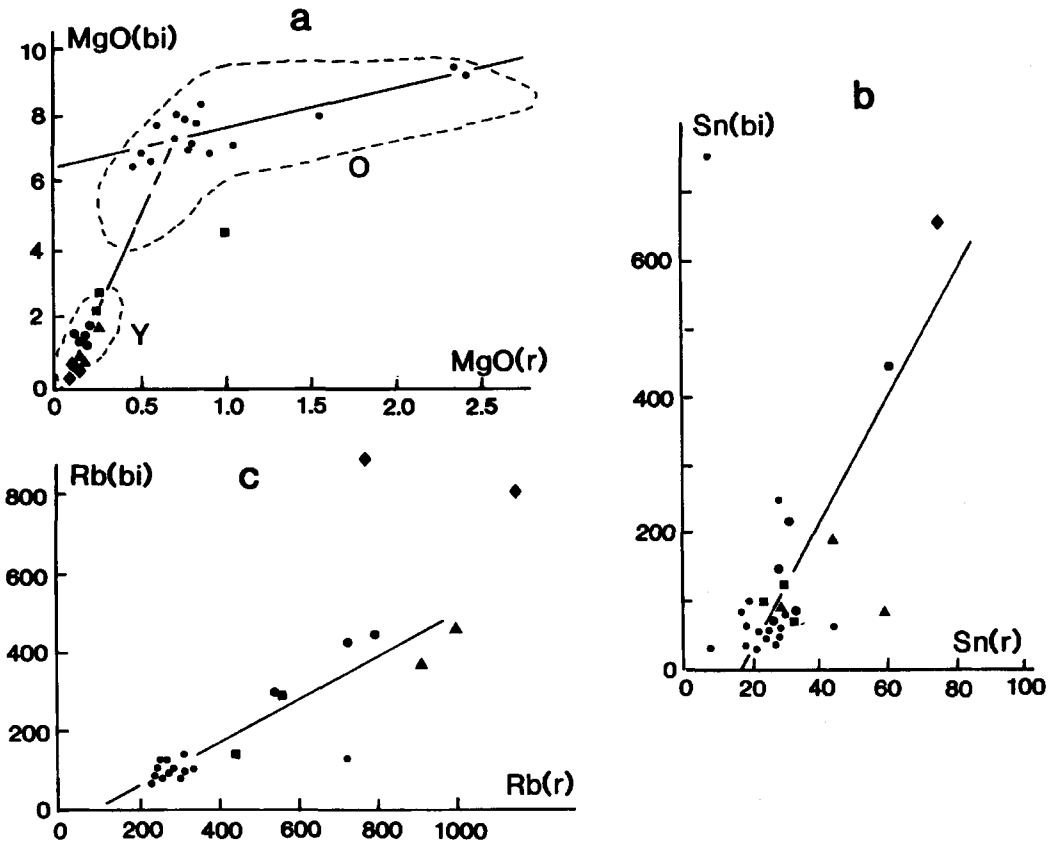

FIG. 5. Mica (bi) *vs.* rock (r) composition diagrams: (*a*) MgO(bi) wt.% *vs.* MgO(r) wt.%; (*b*) Sn(bi) ppm *vs.* Sn(r) ppm; (*c*) Rb(bi) ppm *vs.* Rb(r) ppm.Solid lines are regression lines of Y on X.The steep line in (a) is that of the YIC granites; the other is that of the OIC granites. Fields Y and O (both enclosed in dashed lines) in (a) are the YIC and OIC composition fields for a data set of about 200 partial analyses. Symbols as in Fig. 2. Y on X regressions were made with the aid of the Minitab statistical package: data points situated well away from the main trend (clearly observed by eye) have either large standard residuals or over-influential X-values and have been omitted from the line-fitting.

this would be consistent with high positive correlation between Li and Si (+0.73) and between Fe and Al^{IV} (+0.80); and strong negative correlation between Si and Al^{IV} and between Si and $(Fe^{2+})^{VI}$ (−0.79). On their own, the G3*, G3 and G4 granite biotites define a line with an $Li:Fe^{2+}$ ratio closer to 2:3 and, again, the G2 biotites belong to neither this nor the 1:1 line: the latter is dominated by the Li-micas. However, the Si *vs.* Li diagram, as in Henderson *et al.* (1989, Fig. 4, based upon Cerný and Burt, 1984), takes into account all the ions involved in the coupled substitution in the lithium-iron micas (assuming full octahedral site occupancy). Although our micas would appear to contain more octahedral vacancies, data points plot fairly close to the trend indicated by these authors (Fig. 7*b*): this trend has approximate equations quite close to theirs (their equations 4 and 5, p. 438). The Cornubian data of Stone *et al.* (1988) also follow a similar curve. Indeed, the equation for the data from Karlovy Vary and Stone *et al.* (1988) (n = 52) is

$$2.2Li^{VI} + 0.69Al^{VI} + 1.51Si^{IV} = [2.89R^{2+}]^{VI} + 1.51Al^{IV}$$

where Li has been adjusted to 2.2 for comparison with the equation 5 in Henderson *et al.* (1989). The

TABLE 5. Electron microprobe analyses of Sn in some Cornubian micas

Sample	Mineral	Rock	Range in Sn content	no.	n*	Mean
0653	biotite	B	0 to 130	7	4	<100
0652	biotite	B	30 to 210	7	3	150
0369	biotite	B(CGM)	0 to 120	7	6	<100
0572B	biotite	B	0 to 220	8	5	100
0633	biotite	B(2)	300 to 640	5	0	450
0572A	biotite	A	0 to 180	10	8	<100
0573B	biotite	A	0 to 50	5	5	<100
0566	biotite	A	0 to 80	4	4	<100
0654	biotite	mg	480 to 610	8	0	550
138A	biotite	mg	350 to 390	3	0	350
0651A	biotite	mg	640 to 950	7	0	750
0840	zinnwaldite	E	0 to 100	5	3	<100
0845	muscovite	E(peg)	0 to 5170	6	5	900

Granite type: A = basic microgranite enclave; B = small megacryst granite (outer granite, Carnmenellis pluton); B(2) = as B, but inner granite; B(CGM) = coarse megacrystic granite; mg = late microgranite/aplite dykes; E and E(peg) = lithium-mica granite and pegmatite respectively. n = no. of points counted; n* = no. of points having <100 ppm Sn. The Mean is taken to the nearest 50 ppm above 100 ppm.

equation for all the data considered here (n = 65) is

$$2.2Li^{VI} + 0.85Al^{VI} + 1.36Si^{IV} = [3.04R^{2+}]^{VI} + 1.36Al^{IV}.$$

We assume a single trend here; this is supported by the high correlation coefficient (r = +0.95) and independent line fittings for Karlovy Vary and Cornubian biotite granites and for the Li-mica data sets which show no significant differences either in slope or intercept. Again, many of the biotites plot fairly close to Al-annite with total Al between 3 and 4 and Si between 5 and 6.

The significant correlation between Li_2O and Al_2O_3 (+0.49, Table 2) is dominated by the strong positive covariation of the biotite data, which contrasts with the distinct negative trend shown by the three zinnwaldites, as illustrated by the similar plot for formula Li *vs.* formula total Al (Fig. 4*d*). Henderson *et al.* (1989, Fig. 2*b*) show a distinctly negative relationship here in samples dominated by Li-micas; their two biotite data points stand apart from the rest. This dichotomy in trend shown by the trioctahedral micas is also apparent in the data of Stone *et al.* (1988) and, somewhat less clearly, in the data of Foster (1960*a*). Electron and ion microprobe studies by Henderson *et al.* (1989, Fig. 5) show that in Li *vs.* Al^{VI} plots, the Li-micas follow intra-sample trends > 3 Li:1 Al^{VI}. Inter-sample plots of the three data sets examined here follow similar trends to those of the intra-sample data of Henderson *et al.* (1989), although in Fig. 8, the trend lies almost parallel with the Li axis close to $Al^{VI} = 2$, thereby indicating marked changes in Li at almost constant Al^{VI}. On the other hand, the biotite trend shows a high positive covariation between Li and Al^{VI} up to c. 0.8 atoms of Li and is similar to the trend obtained when Fe^{3+} and Ti are added to Al^{VI}. Thus, there is a change in direction from a biotite trend to a Li-mica trend and substitution in the biotites is

$$Li^{VI} + Al^{VI} + Si^{IV} = [R^{2+}]^{VI} + Al^{IV}$$

as indicated above, whereas that in the Li-micas is

$$Li^{VI} + Si^{IV} = [R^{2+}]^{VI} + Al^{IV}$$

where Li:Fe = 1:1 (Fig. 7*a*) at a constant Al^{VI} of just over 2. Charge differences are balanced by $Si-Al^{IV}$ substitution. Although the trends are dichotomous, two Li-micas lie close to the high Li–high Al^{VI} region of the biotites, suggesting that the change in trend could be continuous and implying that once Al^{VI} reached between 2 and 2.5, there was no more Al admission to the octahedral sites, but only Li substituting for Fe^{2+}, balanced by Si and Al^{IV} adjustment. It may indicate also that the two micas are genetically unrelated in these rocks. This difference in trend is not readily seen in the Si *vs.* Li plot (Fig. 7*b*), presumably because of the presence of octahedral vacancies, the small data sets, and the low obliquity of the Al (and Al^{VI}) lines to the mica trends.

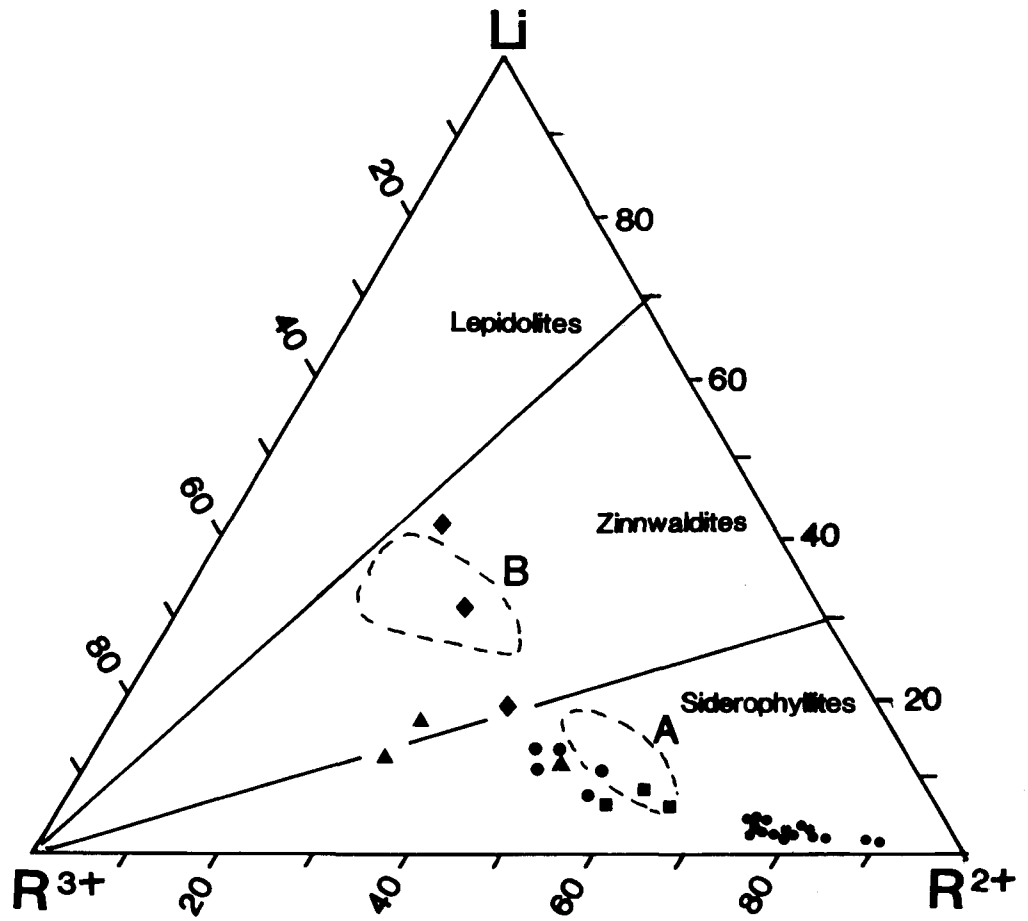

FIG. 6. Octahedral Li-(R^{3+} + Ti)-R^{2+} diagram (after Foster, 1960) showing data points for the Karlovy Vary trioctahedral micas. $R^{3+} = Al^{VI} + Fe^{3+}$, $R^{2+} = Fe^{2+} + Mn$. Symbols as in Fig. 2. Composition fields A and B of Cornubian mica data points as in Fig. 4. Fields for lepidolites, zinnwaldites and siderophyllites after Stone *et al.* (1988).

Comparison with Cornubian trioctahedral micas

A general comparison and petrographic correlation showing many similarities between Cornubian and Karlovy Vary granitoids is given in Rajpoot and Klomínský (1993, 1994) and will not be re-examined in detail here. The principal Cornubian host rocks of the micas examined herein are type B granites (Exley and Stone, 1982) from the small megacryst granites of the Carnmenellis and Isles of Scilly plutons (the Gm granites of Dangerfield and Hawkes, 1981; referred to as G3 by Rajpoot and Klomínský, 1993), type E granites (aphyric zinnwaldite-topaz-albite granites; G5 of Rajpoot and Klomínský, 1993) and late-stage differentiates of the latter (lepidolite-topaz-albite granites). There are many similarities between the YIC biotite-granites and these Cornubian biotite-granites e.g. in TiO_2, tFeO, MgO, CaO, alkalis (including Li), P_2O_5, F, Zr, Rb and the aluminium saturation index (ASI).

Mean compositions of the trioctahedral micas (Table 6) from the main rock types of the Karlovy Vary pluton and those of the Cornubian batholith (Stone *et al.*, 1988) suggest similarities between G3 granite micas and those from the type B granites of SW England. In general, the Cornubian micas are

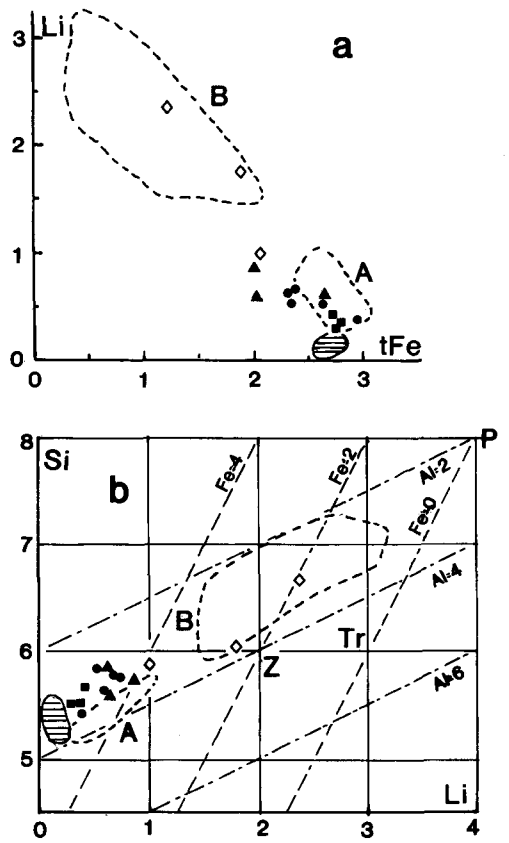

FIG. 7. Bivariate plots to illustrate atomic substitution in the trioctahedral micas. (*a*) Li *vs.* tFe (total Fe as Fe^{2+}); (*b*) Si *vs.* Li. Symbols as in Figs 2 and 4 but with G5 data points now open diamonds. Ruled enclosed area = field of G2 biotites. Composition fields A and B as in Fig. 2. Composition points in 7*b* shown for zinnwaldite (Z), trilithionite (Tr) and polylithionite (P). Al values refer to total Al.

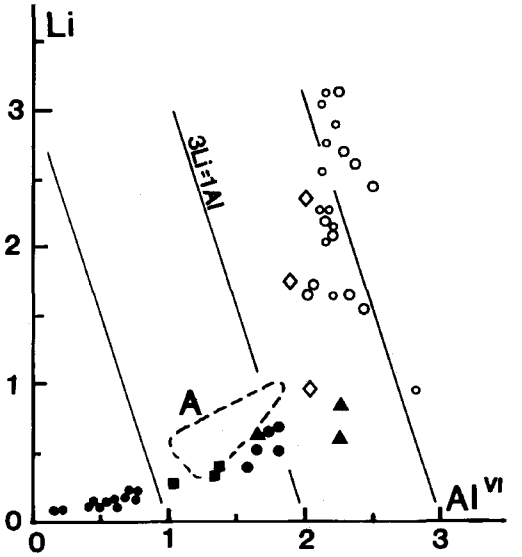

FIG. 8. Li *vs.* Al^{VI} diagram. Field A as in Fig. 4, filled symbols as in Fig. 2 but with open diamonds for G5 micas, small open circles = Li-micas from Henderson *et al.* (1989), large open circles = Li-micas from Stone *et al.* (1988).

richer in Li, Rb and Ni, whereas the Czech micas contain more Sn. Formulae, including octahedral Al and #Fe compare closely. Similarities are also apparent between the zinnwaldites of the G5 granites and those of the albite-topaz-zinnwaldite (type E) granites of S.W. England (cf. Rajpoot and Klomínský, 1993, Table 2). Again, the Cornubian micas are richer in Rb and grade into lepidolite whilst the Czech micas are richer in Sn. Of course, these differences in Rb and Sn may result from using different analytical techniques and calibrations. Apart from these two elements, comparisons are generally close.

Selected data (Fig. 3) illustrate some of the key differences between the trioctahedral micas of the various granite types. Octahedral Al, Si, Li (Fig. 3*e*) and F (Fig. 3*d*) show similar trends in both sets of micas, although the G2 micas have much lower values of #Fe (Fig. 3*f*), F, Li and Al^{VI}. Of course, Al^{IV} has the opposite trend (not shown), as also does Mg (Fig. 3*b*) and tFe^{2+}, with OIC granite micas having the highest values. In several cases (e.g. Al^{VI}, #Fe, Ti, Mg and F), the Cornubian type B granite micas, which are mainly lithian siderophyllites, have compositions that lie between those of the OIC and YIC granite biotites of the Karlovy Vary pluton. Composition fields of the Cornubian micas are indicated in the bivariate plots Li_2O *vs.* SiO_2 (Fig. 2*a*), Li *vs.* F (Fig. 4*a*), F *vs.* Al^{VI}, Al^{VI} *vs.* #Fe (Fig. 4*b*) and Al^{IV} *vs.* #Fe (Fig. 4*c*). Again, these plots and those in Figs 6 and 8 suggest that the YIC biotite-granite micas compare with the type B granite micas (field A) and that the zinnwaldites from both granite masses are comparable (field B). In each case, the OIC granite micas form a separate field in the plots illustrated here. Likewise, in Fig. 7*b* (Si *vs.* Li), there are similarities in plots and closely similar patterns of change between biotites and Li-micas in the two granite sequences that point to broadly similar trends of chemical evolution.

TABLE 6. Average trioctahedral mica compositions

	1	2	3	4	5	6
Wt.%						
SiO_2	34.42	37.58	42.83	36.05	46.42	52.23
TiO_2	3.57	1.57	0.74	2.38	0.60	0.22
Al_2O_3	17.81	22.47	21.96	21.96	21.98	19.74
Fe_2O_3	2.87	3.06	0.87	2.73	1.47	0.29
FeO	18.17	16.96	13.22	19.05	10.48	3.62
MnO	0.41	0.38	0.31	0.41	0.43	1.19
MgO	7.63	1.85	0.51	3.42	0.33	0.18
CaO	0.79	0.36	0.51	0.29	0.17	0.24
Na_2O	0.27	0.32	0.30	0.34	0.83	0.22
K_2O	8.25	8.90	10.88	8.44	9.41	9.30
Li_2O	0.27	0.88	2.96	0.93	3.28	4.95
F	0.76	2.90	6.07	2.16	5.78	6.97
	95.22	97.23	101.16	98.16	101.18	99.15
-O=F	0.32	1.22	2.56	0.91	2.41	2.93
Total	94.90	96.01	98.60	97.25	98.77	96.22
ppm						
Zn	235	389	417	507	394	341
V	175	34	9	180	52	49
Sn	113	148	433	36	66	73
Ga	34	73	52	71	92	82
Cu	14	20	7	5	12	3
Ni	33	8	6	73	81	113
Rb	90	222	563	2145	6504	8653
Formulae						
Si	5.324	5.667	6.191	5.403	6.495	7.152
Al^{IV}	2.676	2.334	1.809	2.597	1.505	0.848
Al^{VI}	0.571	1.659	1.947	1.284	2.124	2.336
Ti	0.416	0.179	0.081	0.268	0.063	0.022
Fe^{3+}	0.334	0.347	0.095	0.302	0.121	0.029
Fe^{2+}	2.351	2.142	1.610	2.390	1.230	0.415
Mn	0.053	0.048	0.038	0.052	0.051	0.138
Mg	1.760	0.416	0.111	0.761	0.070	0.036
Li	0.159	0.532	1.706	0.562	1.846	2.720
ΣY	5.645	5.323	5.558	5.623	5.505	5.697
Ca	0.049	0.024	0.018	0.027	0.000	0.000
Na	0.081	0.094	0.084	0.095	0.224	0.059
K	1.629	1.713	2.010	1.615	1.681	1.623
Rb	0.001	0.002	0.006	0.027	0.064	0.083
ΣX	1.759	1.833	2.118	1.760	1.939	1.764
F	0.373	1.382	2.764	1.025	2.559	3.018
n	16	11	3	11	7	4
Rock type	G2	G3/4	G5	B	E	G

1. Average biotite from G2 granite (from Table 1).
2. Average siderophyllite and lithian siderophyllite from G3/4 granites (from Table 1)
3. Average Li-mica (zinnwaldite) from G5 granite (from Table 1).
4. Average biotite (lithian siderophyllite) from Cornubian type B granite.
5. Average zinnwaldite from Cornubian type E granite.
6. Average lepidolite from Cornubian type G granite.

Cols 4–6 from data in Stone *et al.*, 1988. n = number of samples.*Fe = total Fe/(total Fe + Mg). Al^{IV} = tetrahedral Al; Al^{VI} = octahedral Al.

Petrological significance

Some variation patterns for the Karlovy Vary micas show an apparent continuum between the composition points of biotites in the OIC and YIC granites, e.g. Li_2O *vs.* SiO_2 (Fig. 2*a*), Li *vs.* F (Fig. 4*a*), Li-R^{3+}-R^{2+} (Fig. 6), Li *vs.* tFe and Si *vs.* Li (Fig. 7*b*) suggesting a continuous genetic evolution. However, other comparisons seen in univariate and bivariate plots such as V *vs.* SiO_2 (Fig. 2*c*), Mg and #Fe (Fig. 3) and Al^{IV} *vs.* #Fe (Fig. 4*c*) where OIC granite biotites stand apart from those of the YIC granites, point to contrasting granite suites. In other plots, the two mica sets follow separate trends, e.g. Mg *vs.* tFe (Fig. 4*e*) and mica *vs.* rock plots for MgO (Fig. 5*a*), FeO and TiO_2. This marked separation of the G2 and YIC granite micas is further emphasized by discriminant analysis. The significantly higher TiO_2 contents in both G2 granite and its biotite indicates higher crystallization temperatures (Speer and Becker, 1992; Hecht, 1994; Puziewicz, 1994) than those of the YIC granites which have lower TiO_2 contents in both host rock and biotite.

Štemprok (1992) summarizes geological evidence that strongly favours a double magmatic cycle in the Karlovy Vary pluton. The evidence is provided by: (i) the emplacement of dyke suites that terminate each of the OIC and YIC granite cycles; and (ii) the extrusion of the Teplice rhyolite which separates the two granitic suites. He concludes that the YIC granites were derived from a crustal source already depleted by extraction of OIC granite melts, or from previously solidified OIC granite. The OIC granites have some I-type features (cf. Štemprok, 1992, Fig. 7), they are clearly earlier than the other granites and their trioctahedral micas commonly show discontinuous variation with the other biotite granite micas. The YIC biotite granites have mainly S-type features and their micas show chemical continuity thereby pointing to direct magmatic derivation of G4 from G3. Our evidence for the marked lack of continuity in some constituents between the G2 and YIC granites in their trioctahedral micas and the marked separation in discriminant analysis support the field evidence for a major hiatus. Such a break could occur in a magmatically derived sequence in which the products were episodically emplaced. However, if the time gap between the emplacement of the OIC and YIC granites is 25 Ma (Tischendorf, 1989), a separate origin is more likely. Thus, whilst partial geochemical continuity in these micas implies some consanguinity, the frequent absence of continuity in variation diagrams together with the major multivariate difference indicated by discriminant analysis and the field evidence support the idea of a later separate generation of the YIC biotite granites. We suggest that the YIC biotite granites were derived by direct partial melting of an OIC granite source as indicated by Štemprok (1992), and that their magmas evolved by simple magmatic differentiation from G3 (or G3*) granite to G4 granite along with their biotites.

The Li-mica granites can be interpreted as metasomatically altered biotite granites (cf. Štemprok, 1992) though, in the field, they appear as separate high level Sn-rich plutons. Continuity between biotite and zinnwaldite is indicated in plots presented by Foster (1960), Rieder (1970) and Stone *et al.* (1988) and is supported by some of the data presented herein. Such evidence might suggest continuous evolution of micas (from biotite to Li-mica) and their host rocks and favour simple magmatic processes. However, conflicting evidence is provided by a lack of continuity between Li-micas and the other YIC granite micas in such plots as Rb *vs.* TiO_2 (Fig. 2*b*), tFe and Li (Fig. 3*c* and *e*), Li *vs.* total Al (Fig. 4*d*), Rb(biotite) *vs.* Rb(rock) (Fig. 5*c*). These differences between the micas suggest separate origins and are consistent with evidence from the Cornubian micas (cf. Figs 4*d* and 8 herein) and their host granites (Stone, 1992). In the Cornubian batholith, ultimate differentiation of biotite granite magma leads to biotite microgranites/aplites (in which the biotite shows some enrichment in Rb, F and probably Li), rather than Li-mica granites, although the rocks as a whole show depletion in Cs and Li (Stone, 1992), in marked contrast with the strong enrichment in trace alkalies and F in the Li-mica granites and their micas. Also, the Sn solubility in biotite referred to above (Table 5) increases from biotite granite to later evolved biotite microgranite, but not in trioctahedral micas from a presumed biotite granite–Li-mica granite sequence. We suggest that, like the Cornubian Li-mica granites, the Karlovy Vary host granites may have been derived by melting of a lower crustal biotite-rich residuum immediately following the partial melting of G2 granite that resulted in the production of YIC biotite granite magma, perhaps aided by input of LIL elements from the mantle (Leat *et al.*, 1987; Thorpe, 1987; Stone, 1992), which led to marked enrichment in the trace alkalis and F and the crystallization of Li-micas in place of biotite.

The origin of biotite in these rocks is not directly revealed by its composition, nor that of the host rock. Textural studies of Cornubian granites suggest that, if biotite is magmatic, it crystallized early (Stone, 1979), but that the Li-micas are late magmatic and/or metasomatic (Štemprok, 1986; Stone, 1984; Henderson *et al.*, 1989; Rajpoot, 1992). However, the common field observation of biotite-rich xenoliths passing into streaked-out schlieren and the gradation between these and isolated flakes of biotite indicate that some of the biotite, at least, has been

derived directly from wall rocks at depth or source rocks. Studies of the solubility of biotite in granitoid melts (Puziewicz and Johannes, 1990) suggest again that whilst some biotite can precipitate directly from granitoid melt, much is likely to have been derived as restite material, though thoroughly recrystallized and re-equilibrated with its evolving host magma. On the other hand, Henderson *et al.* (1989) consider that the Li-micas in the Cornubian granites are magmatic in origin, although textural evidence (Stone, 1984) suggests that while lepidolites are magmatic, zinnwaldites exhibit replacement textures and are late magmatic to early postmagmatic.

Acknowledgements

Grateful thanks go to Professor M. Rieder at the Department of Geology, Charles University, Prague, for fruitful discussion. We also thank the British Council, Prague, for a grant that enabled MS to visit the Czech Republic to see these granites in the field and discuss the nature and course of this study. Professor C.M.B. Henderson (University of Manchester) kindly reviewed an early draft and Dr C.S. Exley (University of Keele) kindly reviewed both this and the later manuscript.

References

Bauer, V.H. (1967) Geochemische gliedering granitischer gesteine des Thuringer Waldes und Erzgebirges ihre lagerstatten genetische bedeutung. *Freiberger Forschungshefte* 209.

Cerný, P. and Burt, D.M. (1984) Paragenesis, crystallochemical characteristics and geochemical evolution of micas in granite pegmatites. In *Micas* (S.W. Bailey, ed.) Reviews in Mineralogy, **13**, 257–97. Mineralogical Society of America, Washington.

Chaudhry, M.N. and Howie, R.A. (1973) Lithium-aluminium micas from the Meldon aplite, Devonshire, England. *Mineral. Mag.*, **39**, 289–96.

Dangerfield, J. and Hawkes, J.R. (1981) The Variscan granites of south-west England: additional information. *Proc. Ussher Soc.*, **5**, 116–20.

Exley, C.S. and Stone, M. (1982) Hercynian intrusive rocks. In: *Igneous Rocks of the British Isles*, (D.S. Sutherland, ed.) Wiley, Chichester, 287–320.

Foster, M.D. (1960) Interpretation of the composition of lithium micas. *U.S. Geol. Surv. Prof. Paper*, **354-E**, 115–47.

Gerstenberger, H. (1989) Autometasomatic Rb enrichment in highly evolved granites causing lowered Rb-Sr isochron intercepts. *Earth Planet. Sci. Lett.*, **93**, 65–75.

Gottesmann, B. and Tischendorf, G. (1978) Klassifikation, chemismus und Optik trioktaedrischer Glimmer. *Z. geo. Wiss.*, Berlin, **6**, 681–708.

Haslam, H.W. (1968) The crystallization of intermediate and acid magmas at Ben Nevis, Scotland. *J. Petrol.*, **9**, 84–104.

Hecht, L. (1994) The chemical composition of biotite as an indicator of magmatic fractionation and metasomatism in Sn-specialised granites of the Fichtelgebirge (NW Bohemian Massif, Germany). In *Metallogeny of Collisional Orogens*, (Seltmann, Kämpf and Möller, eds). Czech Geol. Survey, Prague, 295–300.

Henderson, C.M.B., Martin, J.S. and Mason, R.A. (1989) Compositional relations in Li-micas from S.W. England and France: an ion- and electron-microprobe study. *Mineral. Mag.*, **53**, 427–49.

Klomínský, J. and Absolonová, E. (1974) Geochemistry of the Karlovy Vary granite massif (Czechoslovakia). In *Metallization Associated with Acid Magmatism, Vol.* 1 (M. Stemprok, ed.). Geological Survey, Prague, 189–96.

Lange, H., Tischendorf, G., Pälchen, W., Klemm, I. and Ossenkopf, W. (1972) Fortschritte der Metallogenie im Erzgebirge - B, Zur Petrographie und Geochemie der nite des Erzgebirges. *Geologie*, **21**, 457–93.

Leake, B.E. (1974) The crystallization history and mechanism of emplacement of the western part of the Galway granite, Connemara, western Ireland. *Mineral. Mag.*, **39**, 498–513.

Leat, P.T., Thompson, R.N., Morrison, M.A., Hendry, G.L. and Trayhorn, S.C. (1987). Geodynamic significance of post-Variscan intrusive and extrusive potassic magmatism in SW England. *Trans. R. Soc. Edinb.: Earth Sci.*, **77**, 349–60.

Müller, G. (1966) Die Beziehungen zwischen der chemischen Zusammensetzung, Lichtbrechung und Dichte einiger Koexistiezender Biotite, Muskovite und Chlorite aus granitischen Tiefergesteinen. *Contrib. Mineral. Petrol.*, **12**, 173–91.

Neiva, A.M.R. (1976) The geochemistry of biotites from granites of northern Portugal with special reference to their tin content. *Mineral. Mag.*, **40**, 453–66.

Puziewicz, J. (1994) Titanium content in biotite from granitic rocks as an indicator of magma crystallization conditions. *Archiwum Mineralogiczne*, Tom **L**, zeslyt 1, 135–6.

Puziewicz, J. and Johannes, W. (1990) Experimental study of a biotite-bearing granitic system under water-saturated and water-undersaturated conditions. *Contrib. Mineral. Petrol.*, **104**, 397–406.

Rajpoot, G.S. (1992) *Granites in tin metallogenic provinces of Hercynian fold belt (SW England and NW Bohemia) and their comparison with granites in the Himalayas*. Unpubl. PhD thesis, CGU.

Rajpoot, G.S. and Klomínský, J. (1993) Granite in tin fields of Europe and in the Himalayas - a comparative study. *Czech Geol. Surv. Spec. Papers*, **1**, 1–64.

Rajpoot, G.S. and Klomínský, J. (1994) Typology and

origin of granite in the Cornubian and Krušné hory Smrčiny batholiths. *Bull. Czech Geol. Surv.*, **92**, 63–74.

Rieder, M. (1970) Chemical composition and physical properties of lithium-iron micas from the Krušné hory Mts (Erzgebirge). Part A. Chemical composition. *Contrib. Mineral. Petrol.*, **27**, 131–58.

Speer, J.A (1984) Micas in igneous rocks. In *Micas*, (S.W. Bailey, ed.), Mineralogical Society of America, *Reviews in Mineralogy*, **13**, 299–356.

Speer, J.A. and Becker, S.W. (1992) Evolution of magmatic and subsolidus AFM mineral assemblages in granitoid rocks: biotite, muscovite and garnet in the Cuffytown Creek pluton, South Carolina. *Amer. Mineral.*, **77**, 821–33.

Štemprok, M. (1986) Petrology and geochemistry of the Czechoslovak part of the Krušné hory Mts granite pluton. *Sbor. geol. Vèd. Prague, LG*, **27**, 111–56.

Štemprok, M. (1992) Geochemical development of the Krušné hory/Erzgebirge granite pluton exemplified on its Czechoslovak part. *Geophys. Veröff. Univ. Leipzig*, **Bd. IV**, 51–63.

Stone, M. (1979) Textures of some Cornish granites. *Proc. Ussher Soc.*, **4**, 370–9.

Stone, M. (1984) Textural evolution of lithium mica granites in the Cornubian batholith. *Proc. Geol. Assoc.*, **95**, 29–41.

Stone, M. (1992) The Tregonning granite: petrogenesis of Li-mica granites in the Cornubian batholith. *Mineral. Mag.*, **56**, 141–55.

Stone, M., Exley, C.S. and George, M.C (1988) Compositions of trioctahedral micas in the Cornubian batholith. *Mineral. Mag.*, **52**, 175–92.

Thorpe, R.S. (1987) Permian K-rich volcanic rocks of Devon: petrogenesis, tectonic setting and geological significance. *Trans. R. Soc. Edinb.: Earth Sci.*, **77**, 361–6.

Tischendorf, G. (1989) *Silicic magmatism and metallogenesis of the Erzgebirge*. Manuscript, Potsdam, 316 pp.

Tischendorf, G., Frise, G. and Schindler, R. (1969) Die Dunkelglimmer der westerzgebirgisch – vogtländischen Granite und ihre Bedeutung als petrogenetische und metallogenetische Kriterien. *Geologie*, **18**, 1024–44.

Weiss, S. and Troll, G. (1989) The Ballachulish igneous complex, Scotland: petrography, mineral chemistry, and order of crystallization in the monzodiorite – quartz diorite suite and in the granites. *J. Petrol.*, **30**, 1069–115.

[*Manuscript received 4 February 1997: revised 21 May 1997*]